Interactions in Open-Shell Clusters: Ab Initio Study of Pre-reactive Complex $O(^3P) + HCl$[†]

Joanna E. Rode,[‡] Jacek Klos,[‡,§] Lukasz Rajchel,[‡,#] Malgorzata M. Szczesniak,[‡] Grzegorz Chalasinski,[*,#] and Alexei A. Buchachenko[||]

Department of Chemistry, Oakland University, Rochester, Michigan 48309, Faculty of Chemistry, University of Warsaw, Pasteura 1, 02-093 Warszawa, Poland, and Department of Chemistry, Moscow State University, Moscow 119992, Russia

Received: June 23, 2005; In Final Form: October 18, 2005

Van der Waals interactions between the ground-state triplet $O(^3P)$ atom and the closed-shell HCl molecule are investigated in the pre-reactive region. Three adiabatic (two of A″ symmetry and one of A′ symmetry) and four non-relativistic diabatic potential energy surfaces are obtained by combining a restricted open-shell coupled cluster approach with the multireference configuration interaction method. The lower A″ adiabatic potential surface has a single minimum ($D_e = 589$ cm^{-1}) for a linear O···HCl configuration. The upper A″ potential has a weak ($D_e = 65$ cm^{-1}) minimum for a linear HCl···O configuration. The A′ adiabatic potential has a weak (124 cm^{-1}) T-shaped minimum. Adiabatic potentials intersect once in the O···HCl linear configuration and twice in the linear HCl···O geometry. The role of electrostatic interactions in shaping these potentials is discussed. The effects of spin−orbit coupling on this interaction are also investigated assuming a constant value of the SO parameter.

I. Introduction

Reactions involving atoms with nonzero angular momentum proceed on multiple, coupled potential energy surfaces.[1] If such reactions involve potential barriers, the reactants form van der Waals complexes in the reactant valley. These van der Waals minima, which support bound and quasibound states, may trap the reactants before they have a chance to engage in reactive encounters. For example, Skouteris et al.[2] observed that in the $Cl(^2P) + HD$ reaction the presence of a tiny van der Waals well (of ca. 0.5 kcal/mol) in the entrance valley ahead of the 8.5 kcal/mol barrier strongly affects the products distribution. They state, "The fact that such weak van der Waals forces can actually affect the outcome of the reaction is quite remarkable." A frequent occurrence in the pre-reactive region is the crossing of Born−Oppenheimer potential surfaces, which gives rise to nonadiabatic effects. The presence of spin−orbit coupling provides further opportunities for nonadiabatic coupling.[3,4]

We have examined a number of pre-reactive complexes involving ^2P halogens interacting with closed-shell diatomics.[5−9] Ab initio calculations have been employed to characterize the $Cl(^2P) + HCl$,[5] $Cl(^2P) + H_2$,[6] $F(^2P) + H_2$,[7] and $Br(^2P) + H_2$[8] complexes. The results were also reviewed recently.[9] The adiabatic and diabatic potentials derived in these studies were employed in bound-state calculations of Zeimen et al.[10,11]

The subject of this paper is the $O(^3P) + HCl$ van der Waals complex formed in the reactant valley of the reaction between the ground-state $O(^3P)$ and HCl. The $O + HCl \rightarrow OH + Cl$ reaction is of great interest to atmospheric chemistry and serves as a classic example of reaction with heavy−light−heavy dynamics. For these reasons it attracted a great deal of attention from the reactive scattering community (for a recent review see Althorpe and Clary[12]). Recent quantum scattering calculations (on the lowest surface)[13,14] revealed the presence of sharp resonances below the reaction threshold which have been attributed to the presence of the $O(^3P)$−HCl van der Waals wells.

The ground-state potential energy surface (PES) for the $O(^3P) + HCl \rightarrow OH + Cl$ reaction has been the subject of theoretical investigations for a long time. The first reasonable PES of the ground state $^3A''$ was advanced by Koizumi, Schatz, and Gordon (KSG).[15] This PES, which was based on the MP2/6-31G** calculations, was used in numerous quantum calculations of the rate constants (see ref 16 for references). In 1999 Ramachandran et al. developed the multireference configuration-interaction with the approximate correction for quadruples, MRCI+Q/cc-pVTZ, representation of this state.[17] The quasiclassical trajectory calculations on this surface revealed much improvement over the KSG surface, but more accurate quantum calculations suggested that some details were still inaccurate, especially concerning the barrier region.[13,18] Xie et al. used this surface in quantum reactive scattering calculations.[14] They observed a number of low-energy resonances in the cumulative reaction probability of this reaction and concluded that they are related to the quasi-bound states due to the entrance-channel van der Waals complexes. More recently MRCI+Q with a sequence of aug-cc-pVnZ ($n = 2-4$) basis sets by Ramachandran and Peterson[19] generated the lowest energy surfaces for both $^3A''$ and $^3A'$ symmetries. A high level of theory, CBS extrapolation combined with scaling, resulted in what appeared to be the most accurate to date surfaces for the reaction $O(^3P) + HCl \rightarrow OH + Cl$. Their potential contains van der Waals wells on both the product and reactant sides of the barrier.

All the potential energy surfaces mentioned thus far map the total Born−Oppenheimer energy of a dimer as a function of geometry. In this representation, the energy does not approach

[†] Part of the special issue "Jack Simons Festschrift".

* Corresponding author. E-mail: chalbie@tiger.chem.uw.edu.pl.
[‡] Oakland University.
[§] Present address: Department of Chemistry and Biochemistry, University of Maryland, College Park, MD 20742-2021.
[#] University of Warsaw.
[||] Moscow State University.

10.1021/jp053419q CCC: $30.25
Published on Web 12/15/2005

zero as the monomers become infinitely separated. In the entrance channel, where the monomers are well defined, it is advantageous to map the *interaction* energy as a function of geometry. Such *interaction* potential energy surfaces reflect the forces between approaching reactants, which, in the case of open-shell moieties, are still incompletely understood. They are also convenient for discussing the effect of the spin−orbit coupling, and especially, for the calculations of bound states. The goal of this paper is to characterize the forces in the pre-reactive region of the O(^{3}P) + HCl reaction by calculating three interaction potential energy surfaces, $1^3A''$, $2^3A''$, and $^3A'$, which result from the splitting of the ^{3}P term due to the interaction with HCl.

Calculations of interaction energies in the case of multiple, coupled potential surfaces are far from trivial. In the MRCI method the main impediment is the size-nonextensivity. The approximate size-consistency corrections involving correcting for quadruples (MRCI+Q), though relatively accurate with respect to total energies, are insufficiently accurate with respect to (several orders of magnitude smaller) interaction energies. To circumvent this problem, the MRCI+Q dimer calculations customarily refer to the asymptotic limit obtained from a dimer calculation at some artificially large separation, rather than to two separately calculated monomer energies.[20] However, such an approach hinders the application of counterpoise corrections that require the calculations of monomer energies in the basis set of the whole dimer.[21] Within the MRCI framework the separate monomers cannot be defined in a consistent manner. Second, the MRCI method requires several more or less arbitrary choices, such as a partitioning into core, inactive, and active orbitals, making it impossible to design a sequence of convergent calculations with respect to the one-electron basis set and model space extensions. Third, MRCI is not as efficient as the coupled cluster treatment with single, double, and noniterative triple excitations (CCSD(T)) in the treatment of dispersion-dominated van der Waals interactions. Our results indicate[5] that in the Cl + HCl complex the dispersion energy may be underestimated by the MRCI by as much as 30% due to the absence of triple excitations.

The most accurate approach is the open-shell CCSD(T) treatment applied in the partially spin restricted (RCCSD(T)) framework. This approach is size-extensive, and due to the inclusion of triple excitations, highly accurate in treating the dispersion-bound complexes. It is, however, limited to the instances where the single Hartree−Fock determinant represents a reasonable first approximation. In the O(^{3}P)−HCl interaction there are two singly occupied and one doubly occupied orbital in the O atom corresponding to the ground ^{3}P term, which in the absence of the spin−orbit coupling, is triply degenerate. Interaction with HCl removes this degeneracy, giving rise to three states, which differ by the orientation of the doubly occupied p orbital (see Figure 1 for the description of the coordinate system). In the C_s group the two lowest $^3A''$ states correspond to the doubly occupied orbital lying in the triatomic plane, whereas the $^3A'$ state the doubly occupied orbital is perpendicular to this plane. In the linear $C_{\infty v}$ geometry, the $^3\Sigma^-$ state is represented by the doubly occupied orbital pointing toward HCl, and the $^3\Pi$ state corresponds to its perpendicular orientations. According to Szalay and Gauss,[21] such are the circumstances where both the ground state and the first excited state of the same symmetry can be treated by the single reference approach: a restricted open-shell coupled-cluster method. Another factor is that these states are split by an appreciable electrostatic interaction of the quadrupole moment of the O(^{3}P) atom with the dipole and quadrupole moments of HCl. Of course, the rigorous treatment of the coupling between these states requires the application of the multireference approaches, such as MRCI.

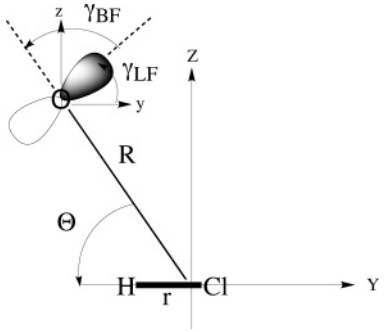

Figure 1. Coordinate systems for O(^{3}P) + HCl calculations. The angle γ describes the orientation of the doubly occupied 2p orbital of O(^{3}P) in either the laboratory-fixed (LF) or body-fixed (BF) coordinate system (see the text).

In this paper the three interaction potential energy surfaces, $1^3A''$, $2^3A''$, and $^3A'$ (among which two are coupled) will be obtained using the approach that combines RCCSD[T] for the evaluation of interaction energies and the MRCI method for nonadiabatic coupling. The latter term is necessary to carry out a transformation to a diabatic representation. The electrostatic character of this coupling will be investigated, as well as the effects of the spin−orbit coupling on the structure and energetics of this interaction.

II. Details of ab Initio Calculations

The Cartesian and Jacobi coordinates for O + HCl are shown in Figure 1. The linear molecule HCl lies along the *y* axis. *yz* is the triatomic plane. The intermolecular vector from the center of mass of the molecule to the atom is denoted **R** and the intramolecular vector is **r**. The angle between the unit vectors of **R** and **r** is denoted Θ. The potentials advanced in this work assumed the constant $r = 1.275$ Å. In section III.4 the effects of variation of *r* on the state crossing will also be discussed.

Three Born−Oppenheimer (adiabatic) potentials $V_{1A''}$, $V_{2A''}$, and $V_{A'}$ were calculated using the RCCSD[T] method with the aug-cc-pVQZ basis set. Selected calculations for linear configurations included bond functions. Six orbitals were included in the frozen core (1 on O, 5 on Cl) in both RCCSD[T] and MRCI calculations.

Interaction potentials V were obtained within the supermolecular approach and corrected for the BSSE using Boys−Bernardi counterpoise (CP) procedure.[20] In the open-shell monomer case, the presence of the ghost orbitals splits the ^{3}P atomic term into three monomer states.[22] These states were correlated with the dimer states of the appropriate symmetry. All electronic calculations were carried out using the *Molpro* suite of programs.[23]

The adiabatic solutions are not appropriate for scattering and dynamics calculations and it is customary to transform them into a diabatic representation. Dynamic calculations require additional information beyond that contained in the adiabatic potentials, such as the nonadiabatic couplings. Diabatic states can be obtained by a unitary transformation of the adiabatic states, which for a case of two same-symmetry states can be determined by the single adiabatic-to-diabatic transformation angle γ[24] (also referred to as the mixing angle). The resulting diabatic potential matrix is not diagonal and the off-diagonal

potential surface, which is necessary for bound-state and scattering calculations, can also be related to the mixing angle γ.[20,25]

The mixing angle was obtained in parallel MRCI/aug-cc-pvQZ calculations of the three states. They were used in subsequent calculations to evaluate the transition moments of the L_y component of the angular momentum operator. The mixing angle calculations do not involve any energy differences; therefore, there is no need for size-extensivity and BSSE corrections. The three-state averaged CASSCF that preceded the internally contracted MRCI[26] included eight active orbitals (6 a′ and 2 a″). The laboratory-frame (LF) mixing angle is then obtained from (see ref 25 for details)

$$\gamma_{\mathrm{LF}} = \arctan\frac{\langle 1\mathrm{A}'|L_y|1\mathrm{A}''\rangle}{\langle 1\mathrm{A}'|L_y|2\mathrm{A}''\rangle} \tag{1}$$

Transformation to a diabatic basis yields the four potential energy surfaces

$$\begin{aligned} H_{11} &= V_{1\mathrm{A}''}\cos^2\gamma_{\mathrm{BF}} + V_{2\mathrm{A}''}\sin^2\gamma_{\mathrm{BF}} \\ H_{22} &= V_{1\mathrm{A}''}\sin^2\gamma_{\mathrm{BF}} + V_{2\mathrm{A}''}\cos^2\gamma_{\mathrm{BF}} \\ H_{12} &= H_{21} = (V_{1\mathrm{A}''} - V_{2\mathrm{A}''})\cos\gamma_{\mathrm{BF}}\sin\gamma_{\mathrm{BF}} \\ H_{33} &= V_{\mathrm{A}'} \end{aligned} \tag{2}$$

where γ_{BF} denotes the mixing angle transformed from LF to body-fixed (BF) coordinate system (see Figure 1).

In the long-range part of the potential energy surfaces the interactions are dominated by electrostatics. This role of the electrostatic contributions was first recognized by Rebentrost and Lester.[27] Dubernet and Hutson[28] pointed out that *both* the relative magnitude of electrostatic anisotropy and the SO splitting affect the bending dynamics of a diatomic molecule in such complexes.

The electrostatic interaction, through the R^{-5} terms, in the diabatic representation was calculated from the following expressions:[11]

$$\begin{aligned} H_{11}^{\mathrm{es}} &= 3P_1^0(z)Q_{\mathrm{O}}\mu_{\mathrm{HCl}}/R^4 + 6P_2^0(z)Q_{\mathrm{O}}Q_{\mathrm{HCl}}/R^5 \\ H_{22}^{\mathrm{es}} &= -{}^3/_2P_1^0(z)Q_{\mathrm{O}}\mu_{\mathrm{HCl}}/R^4 + [-3P_2^0(z) + {}^1/_4P_2^2(z)]Q_{\mathrm{O}}Q_{\mathrm{HCl}}/R^5 \\ H_{33}^{\mathrm{es}} &= -{}^3/_2P_1^0(z)Q_{\mathrm{O}}\mu_{\mathrm{HCl}}/R^4 + [-3P_2^0(z) - {}^1/_4P_2^2(z)]Q_{\mathrm{O}}Q_{\mathrm{HCl}}/R^5 \\ H_{12}^{\mathrm{es}} &= {}^3/_2P_1^1(z)Q_{\mathrm{O}}\mu_{\mathrm{HCl}}/R^4 + 2P_2^1(z)Q_{\mathrm{O}}Q_{\mathrm{HCl}}/R^5 \end{aligned} \tag{3}$$

where $P_k^l(z)$ are the associated Legendre functions in $z = \cos\Theta$. The dipole and quadrupole moments of HCl molecule were calculated at CCSD[T]/aug-cc-pVQZ level and set to $\mu_{\mathrm{HCl}} = 0.469$ au and $Q_{\mathrm{HCl}} = 2.754$ au (experimental value 2.75 au), respectively. The value of the quadrupole moment of the oxygen atom was taken from the work of Medved et al.[29] and was equal to $Q_{\mathrm{O}} = -1.036$ au. The electrostatic representation of the two A″-symmetry adiabats V_1^{es} and V_2^{es} was obtained by the diagonalization of the above electrostatic diabats. In the long range, $R > 5.5$ Å, the ab initio values for the diabatic potentials were extrapolated from the electrostatic formulas.

III. Results and Discussion

1. Ab Initio Interaction Energies and PESs. The adiabatic $V_{1\mathrm{A}''}$ and $V_{2\mathrm{A}''}$ potential energy surfaces are presented in Figure 2. The minimum characteristics are summarized in Table 1. The $V_{1\mathrm{A}''}$ adiabat has a single minimum at the linear configuration $\Theta = 0°$ (hydrogen-bonded configuration) with the well depth

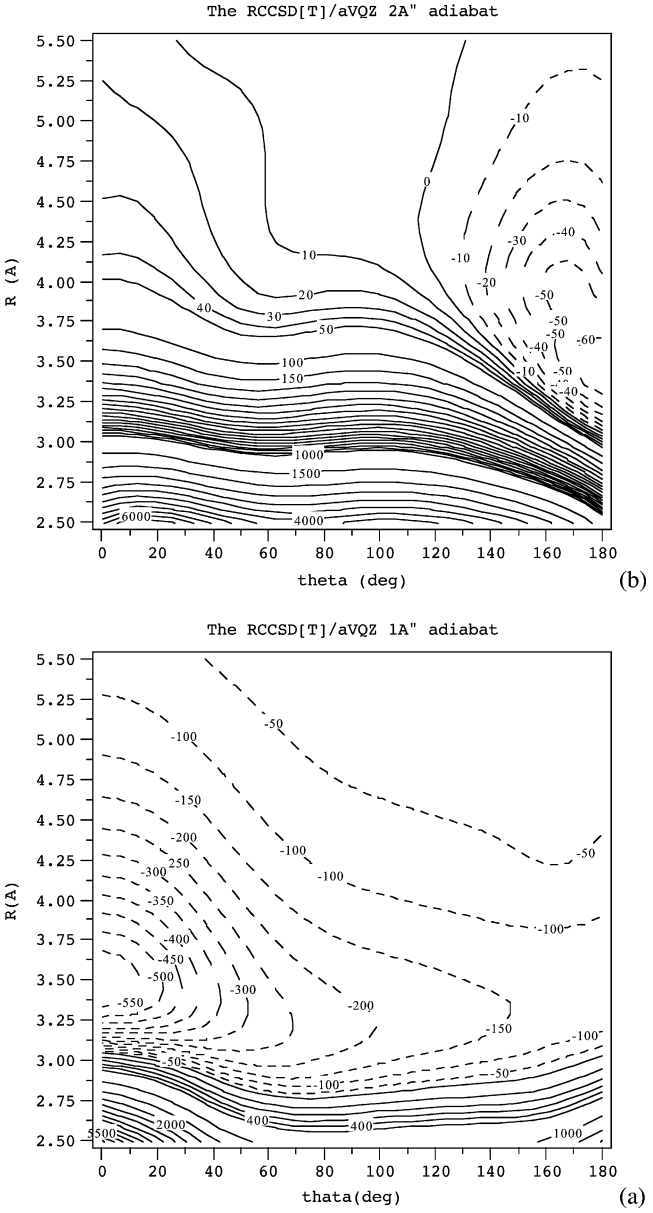

Figure 2. Adiabatic potentials for O + HCl (dashed contours represent attractive energies): (a) $1^3\mathrm{A}''$; (b) $2^3\mathrm{A}''$.

TABLE 1: O(^{3}P) + HCl Well Depths of the Three Adiabatic ($V_{1\mathrm{A}''}$, $V_{2\mathrm{A}''}$, $V_{\mathrm{A}'}$) and Three Diabatic (H_{11}, H_{22}, $V_{\mathrm{A}'} = H_{33}$) PESs from ab Initio Calculations; Energy Values in cm^{-1}

Θ (deg)	R (Å)	RCCSD[T])/ avqz	RCCSD[T]/ avqz+332211 bf	MRCI+Q/CBS[a]
		$V_{1\mathrm{A}''}$		
0	3.50	589	595	538
		$V_{2\mathrm{A}''}$		
180	3.45	65	74	
		$V_{\mathrm{A}'} = H_{33}$		
100	3.50	124		
		H_{11}		
0	3.50	589	595	
180	3.45	144	151	
		H_{22}		
90	3.25	203		

[a] From ref 19.

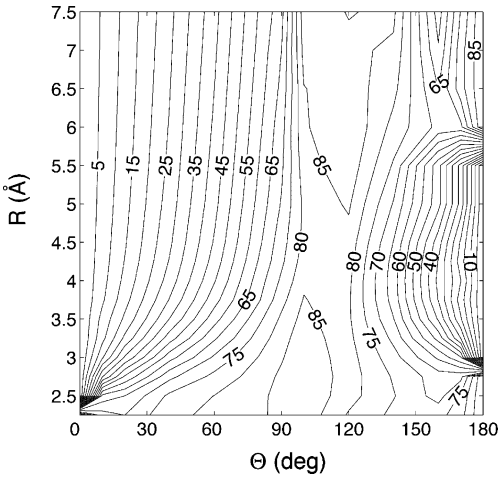

Figure 3. Adiabatic-to-diabatic transformation angle γ_{BF} from MRCI calculations.

of ca. 589 cm^{-1} at $R = 3.5$ Å. In this minimum, the doubly occupied orbital of O points toward H and in the $C_{\infty v}$ group corresponds to a $^3\Sigma^-$ state. The upper adiabat has a shallow non-hydrogen-bonded minimum at $\Theta = 180°$ with the well-depth of ca. 65 cm^{-1} at the same distance. For the global minimum, additional calculations employed bond functions that included 3s, 3p, 2d, 2f, 1g, 1h Gaussians (denoted 332211) placed in the *R* midpoint. Bond functions are known to improve the description of the dispersion interaction.[30] The well depth increased by only 6 cm^{-1}. The third adiabat $V_{A'}$ has the single T-shaped minimum. This potential remains the same upon diabatization and will be shown below.

2. Transformation to Diabatic Basis. In the present case the CASSCF and MRCI calculations led to a very similar description of the geometry-dependence of the adiabatic-to-diabatic transformation angle. The results for $\gamma_{BF}(R,\Theta)$ presented in Figure 3 were obtained by the MRCI method. For the purposes of the analysis that follows, the angle has been reduced to the first quarter. However, such a procedure leads to the loss of information about the sign of the off-diagonal coupling term.

The extreme mixing-angle values, 0° and 90°, correspond to zero coupling, i.e., to the pure noninteracting states. The 45° angle corresponds to the maximal coupling that results either in the degeneracy (a conical intersection) or in an avoided crossing. Two characteristic features of the mixing angle are noticeable. In the vicinity of H-bonded geometry ($\Theta = 0°$), there is a single short-range conical intersection. At this point an avoided crossing originates and continues toward the bent geometries with $\Theta = 60°$ in the asymptotic region. In the vicinity of the non-H-bonded geometries ($\Theta = 180°$) the avoided crossing forms a loop connecting the two conical intersections: a short-range and a long-range one. In section III.4 we will discuss how these crossings behave when the HCl bond distance *r* is varied.

Diabatic potentials are shown in Figures 4 and 5. The H_{11} diabat has a double-minimum character with the deeper minimum for the H-bonded configuration (with the same well depth as $V_{1A''}$). The H_{22} diabat has a single minimum for the T-shaped configuration, and its well depth is 203 cm^{-1} at $R =$ 3.25 Å. The H_{33} potential that is the same as $V_{A'}$ adiabat is shown in Figure 5. The characteristics of minima in both representations are summarized in Table 1. The off-diagonal potential H_{12} has a simple wavelike shape with the attractive region for $\Theta < 100°$ and the repulsive one for $\Theta > 100°$. The nature of this potential is revealed when we examine the

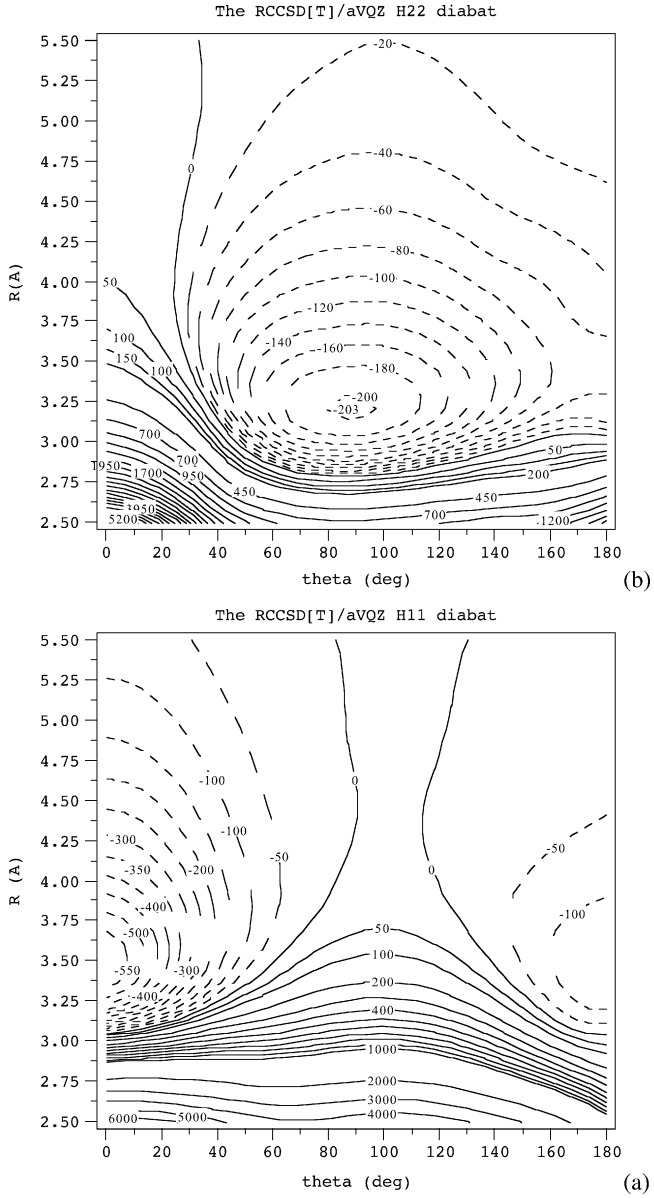

Figure 4. Diabatic potentials for O + HCl (dashed contours represent attractive energies): (a) H_{11} diabat; (b) H_{22} diabat.

electrostatic H_{12}^{es} obtained using eq 3, as shown in Figure 6. The ab initio and electrostatic H_{12} (cf. Figure 5b and 6) are remarkably similar, leading us to the conclusion that H_{12} has a predominantly electrostatic origin.

3. Electrostatic Treatment of Long-Range Potentials. As discussed in the context of the mixing angle (Figure 3), on the non-H-bonded side there are two conical intersections. The regions beyond the more distant conical intersection ($R > 6$ Å, $\Theta = 180°$) are particularly demanding computationally. The two surfaces are only a few cm^{-1} apart, and the RCCSD[T] method fails. The MRCI method is also difficult to apply because the reference wave function changes rapidly in the proximity of this conical intersection. Fortunately, at these distances one can expect the electrostatic interactions to dominate. The electrostatic diabats H_{11}^{es} and H_{22}^{es} and H_{12}^{es} were obtained from eq 3 along with the respective adiabats, V_1^{es} and V_2^{es}, from their diagonalization. The resulting cross-section of the PESs at $R = 5.5$ Å is displayed in Figure 7. A comparison with the respective ab initio CASSCF values indicates that the electrostatic approximation involving dipole−quadrupole + quadrupole-quadrupole terms is satisfactory and it can be used

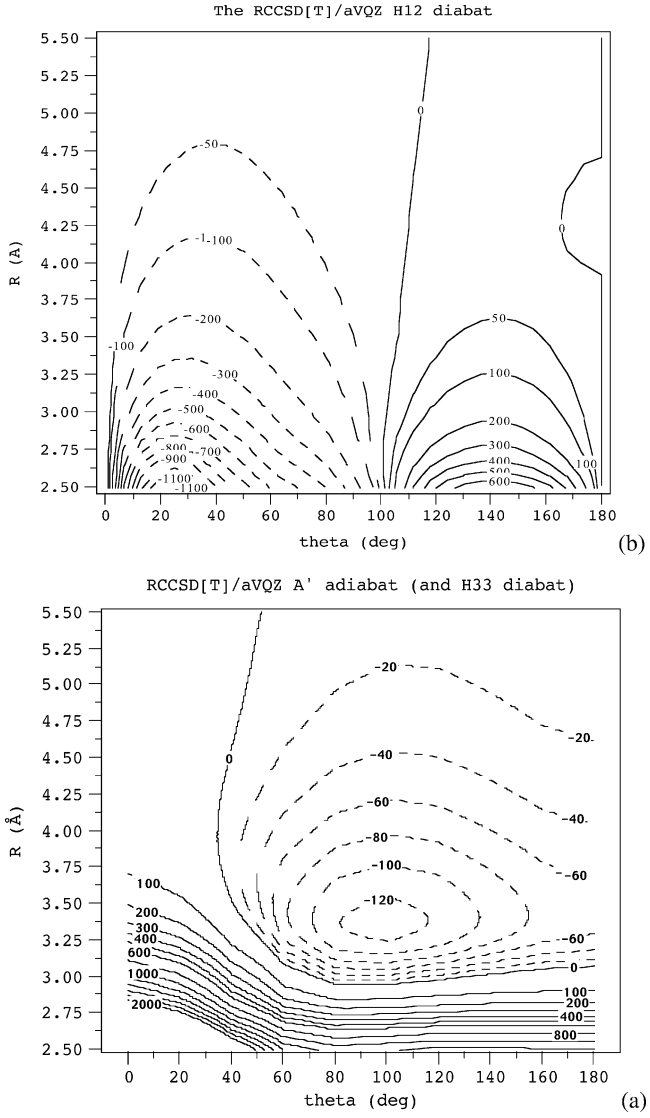

Figure 5. Diabatic potentials for O + HCl (dashed contours represent attractive energies): (a) H_{33} diabat equivalent to the adiabatic potential $^3A'$; (b) H_{12} diabatic potential from ab initio calculations.

to reliably extrapolate potential surfaces in the long range. The qualitative agreement between the ab initio and electrostatic representations of the off-diagonal diabatic potential term H_{12} is particularly noteworthy.

4. Linear Geometries and the *r* Variation. In linear $C_{\infty v}$ geometry there are two states, $^3\Sigma^-$ and $^3\Pi$. In the H-bonded configuration ($\Theta = 0°$) the $^3\Sigma^-$ state lies below the repulsive $^3\Pi$ state (see Figure 8 bottom panel). In Cl(^{2}P) + HCl[5] (see Figure 8 upper panel) the order of states is reversed, but the shapes of the two states are strikingly similar. In both complexes there is a single crossing at short distances (see section III.2): at $R = 2.6$ Å in O + HCl and $R = 3.1$ Å in Cl + HCl. On the non-H-bonded side ($\Theta = 180°$) in O + HCl both $^3\Sigma^-$ and $^3\Pi$ states have minima and $^3\Sigma^-$ is deeper. In the Cl + HCl complex the $^2\Sigma$ and $^2\Pi$ states are reversed, and the shapes of the curves are again similar (see Figure 8 upper panels). In both cases the states cross twice: once in the short range and the second time in the long range.

It is interesting to explore how the conical intersections behave with respect to the increase of the H−Cl bond distance *r*. The coordinate *r* was varied from the equilibrium to 1.63 Å. Two issues were addressed in this context. The first involved comparing the Σ and Π intersections of the *total* dimer energies

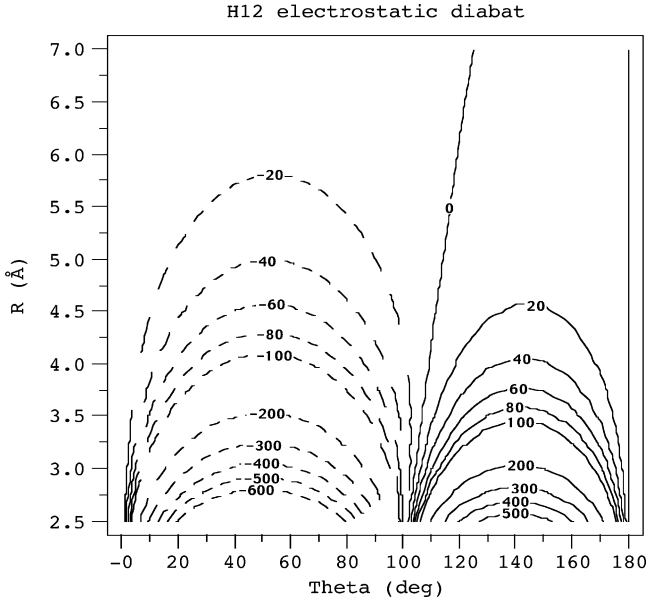

Figure 6. H_{12} diabatic potential from electrostatic expression (dashed contours represent attractive energies).

vs the intersections of the *interaction* potentials. The picture is very similar in both representations. There are two crossings in both cases and their locations are roughly the same. The *r*-dependence of the two crossing states is shown in Figure 9. The short-range intersection shifts toward the shorter *R* as *r* increases. The long-range intersection remains at the same distance, ca. $R = 5.75$ Å, as *r* increases. To summarize, stretching H−Cl by up to 25% maintains the presence of the two conical intersections on the non-H-bonded side.

5. Spin−Orbit Coupling. In O(^{3}P) + HCl complex the O(^{3}P) atom is the source of orbital λ and spin **S** angular momentum. The total electronic angular momentum of a spin−orbit coupled state will be denoted $\mathbf{J} = \lambda + \mathbf{S}$. The orbital (complex) basis set $|\lambda\mu\rangle$ (see Zeimen et al.[11] for more details) in the present case involves $\lambda = 1$ and $\mu = -1, 0, +1$. We first describe potential matrix elements in this complex basis set ($\lambda = 1$ is omitted for simplicity) using diabatic potentials, H_{11}, H_{22}, H_{33}, and H_{12}, expressed in the real Cartesian basis of p_x, p_y, and p_z obtained above. It is convenient to use abbreviated notations: V_Σ, V_Π, V_1, and V_2.

$$V_\Sigma = \langle 0|V|0\rangle = H_{11}$$

$$V_\Pi = \langle 1|V|1\rangle = \langle -1|V|-1\rangle = {}^1/_2(H_{33} + H_{22})$$

$$V_2 = \langle 1|V|-1\rangle = \langle -1|V|1\rangle = {}^1/_2(H_{33} - H_{22})$$

$$V_1 = \langle 0|V|1\rangle = -\langle 0|V|-1\rangle = -\frac{1}{\sqrt{2}}H_{12} \qquad (4)$$

In this section the treatment of the SO coupling will be discussed in the $\lambda\mathbf{S}$-coupled and uncoupled basis sets. We begin with the coupled $|JM_J\rangle$ basis set:

$$|JM_J\rangle = \sum_{\mu,\sigma}\langle\lambda\mu S\sigma|JM_J\rangle|\lambda\mu\rangle|S\sigma\rangle \qquad (5)$$

where the $\langle\ |\ \rangle$ symbols denote Clebsch−Gordan coefficients, *J* is equal to 0, 1, 2, and $|M_J| = 0, ..., J$. The parity-adapted $|JM_J\rangle$ basis set takes the form

$$|J|M_J|\epsilon\rangle = \frac{1}{\sqrt{2(1+\delta_{M_J,0})}}(|JM_J\rangle + \epsilon|J-M_J\rangle) \qquad (6)$$

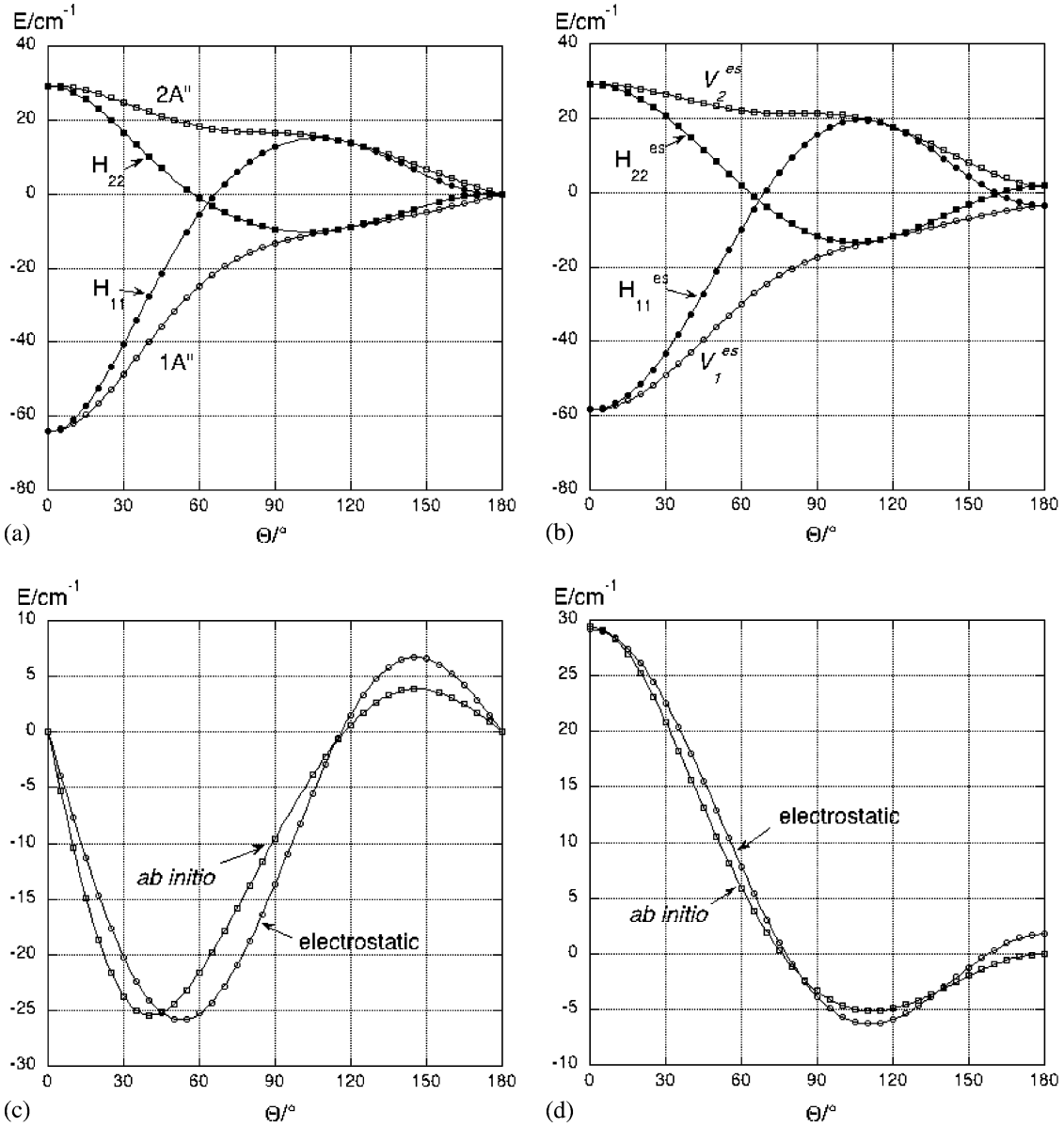

Figure 7. Comparison between ab initio (adiabats from the CASSCF calculations and the mixing angle from MRCI) and electrostatic calculations of the diabatic and adiabatic states at $R = 5.5$ Å: (a) ab initio adiabatic and diabatic potentials; (b) electrostatic adiabatic and diabatic potentials; (c) off-diagonal diabatic term H_{12}; (d) $H_{33} = V_{A'}$ potential.

where ϵ denotes the parity index related to parity $p = \epsilon(-1)^J$. The parity-adapted basis set is

$$|22+\rangle = \frac{1}{\sqrt{2}}(|11\rangle + |-1-1\rangle)$$

$$|22-\rangle = \frac{1}{\sqrt{2}}(|11\rangle - |-1-1\rangle)$$

$$|21+\rangle = {}^1/_2(|10\rangle + |01\rangle + |-10\rangle + |0-1\rangle)$$

$$|21-\rangle = {}^1/_2(|10\rangle + |01\rangle - |-10\rangle - |0-1\rangle)$$

$$|11+\rangle = {}^1/_2(|10\rangle - |01\rangle + |0-1\rangle - |-10\rangle)$$

$$|11-\rangle = {}^1/_2(|10\rangle - |01\rangle - |0-1\rangle + |-10\rangle)$$

$$|20\rangle = 1/\sqrt{6}(|1-1\rangle + 2|00\rangle + |-11\rangle)$$

$$|10\rangle = 1/\sqrt{2}(|1-1\rangle - |-11\rangle$$

$$|00\rangle = 1/\sqrt{3}(|1-1\rangle - |00\rangle + |-11\rangle \quad (7)$$

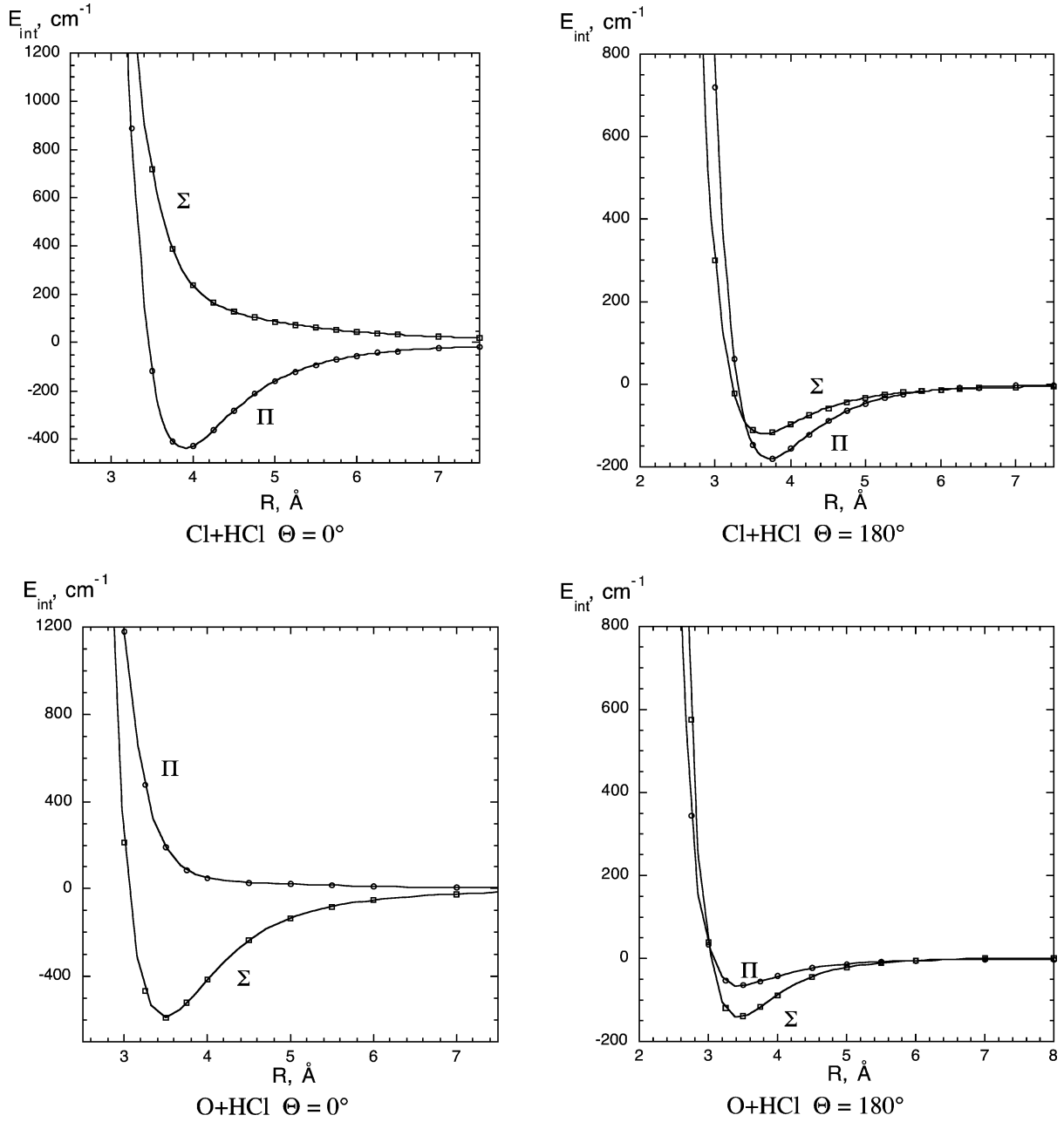

Figure 8. Comparison of the $C_{\infty v}$ interaction potentials for O(^{3}P) + HCl (bottom panels) and Cl(^{2}P) + HCl (upper panels; data from ref 5).

where the kets on the right-hand side show the μ,σ values. In the coupled basis set the spin−orbit Hamiltonian $H_{SO} = a\lambda\cdot\mathbf{S}$ is diagonal. The spin−orbit parameter $a = -77.47$ cm^{-1} [31] was assumed to be constant across the whole region of R and Θ. In this parity-adapted $\lambda\mathbf{S}$-coupled basis set $V + H_{SO}$ is represented by the 9×9 symmetric matrix, whose rows and columns are numbered with $|22+\rangle$, $|21+\rangle$, $|11+\rangle$, $|20\rangle$, $|00\rangle$, $|22-\rangle$, $|21-\rangle$, $|11-\rangle$, $|10\rangle$:

$$\begin{bmatrix}
V_\Pi + a & 0 & -\frac{1}{\sqrt{2}}V_1 & \frac{1}{\sqrt{3}}V_2 & \frac{2}{\sqrt{6}}V_2 & 0 & \frac{1}{\sqrt{2}}V_1 & 0 & 0 \\
 & \frac{1}{2}(V_\Pi + V_2 + V_\Sigma) + a & 0 & 0 & 0 & \frac{1}{\sqrt{2}}V_1 & 0 & \frac{1}{2}(V_\Pi + V_2 - V_\Sigma) & \frac{1}{\sqrt{2}}V_1 \\
 & & \frac{1}{2}(V_\Pi - V_2 + V_\Sigma) - a & \frac{3}{\sqrt{6}}V_1 & 0 & 0 & \frac{1}{2}(V_\Pi + V_2 - V_\Sigma) & 0 & 0 \\
 & & & \frac{1}{3}(V_\Pi + 2V_\Sigma) + a & \frac{\sqrt{2}}{3}(V_\Pi - V_\Sigma) & 0 & \frac{1}{\sqrt{6}}V_1 & 0 & 0 \\
 & & & & \frac{1}{3}(2V_\Pi + V_\Sigma) - 2a & 0 & -\frac{2}{\sqrt{3}}V_1 & 0 & 0 \\
 & & & & & V_\Pi + a & 0 & -\frac{1}{\sqrt{2}}V_1 & -V_2 \\
 & & & & & & \frac{1}{2}(V_\Pi - V_2 + V_\Sigma) + a & 0 & 0 \\
 & & & & & & & \frac{1}{2}(V_\Pi + V_2 + V_\Sigma) - a & -\frac{1}{\sqrt{2}}V_1 \\
 & & & & & & & & V_\Pi - a
\end{bmatrix} \tag{8}$$

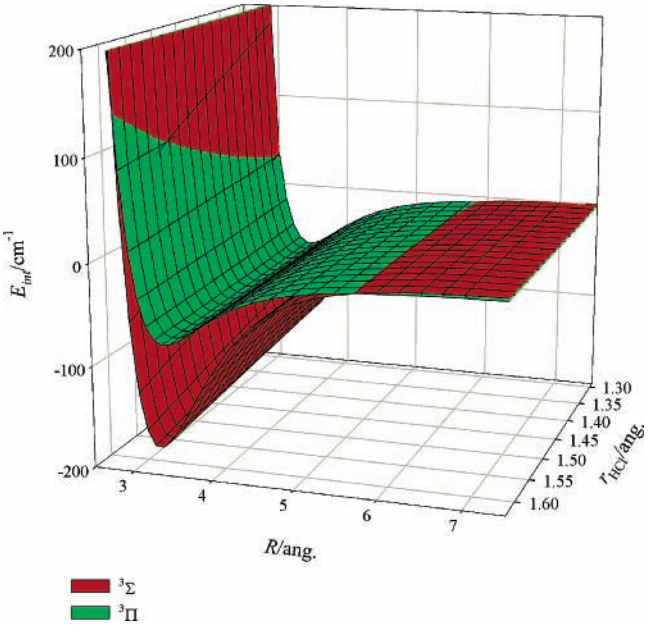

Figure 9. Crossing of the $^3\Sigma$ and $^3\Pi$ interaction potentials of O + HCl (non-H-bonded geometry: $\Theta = 180°$) as a function of the HCl intramonomer coordinate *r*.

The spin−orbit coupling can also be treated in the uncoupled basis set $|\lambda\mu S\sigma\rangle$. This treatment was applied previously to O(^{3}P) + rare gases by Buchachenko et al.[32] In this representation the H_{SO} operator is not diagonal:

$$\langle\lambda\mu S\sigma|\hat{H}_{SO}|\lambda\mu' S\sigma\rangle = a\delta_{\sigma\sigma'}\langle\lambda\mu|\hat{l}_z\hat{s}_z + {}^1/_2\hat{l}_+\hat{s}_- + {}^1/_2\hat{l}_-\hat{s}_+|\lambda\mu'\rangle \quad (9)$$

where the ladder operators have the following eigenvalues

$$\langle\lambda\mu|\hat{l}_\pm|\lambda\mu'\rangle = \sqrt{\lambda(\lambda+1) - \mu'(\mu'\pm 1)}\,\delta_{\mu\mu'\pm 1}$$

$$\langle S\sigma|\hat{s}_\pm|S\sigma'\rangle = \sqrt{S(S+1) - \sigma'(\sigma'\pm 1)}\,\delta_{\sigma\sigma'\pm 1} \quad (10)$$

In this basis set $V + H_{SO}$ is also represented by the 9 × 9 symmetric matrix, whose rows and columns are numbered with $|1{-}11{-}1\rangle$, $|1{-}110\rangle$, $|1{-}111\rangle$, $|101{-}1\rangle$, $|1010\rangle$, $|1011\rangle$, $|111{-}1\rangle$, $|1110\rangle$, $|1111\rangle$:

$$\begin{bmatrix} V_\Pi + a & 0 & 0 & -V_1 & 0 & 0 & V_2 & 0 & 0 \\ & V_\Pi & 0 & a & -V_1 & 0 & 0 & V_2 & 0 \\ & & V_\Pi - a & 0 & a & -V_1 & 0 & 0 & V_2 \\ & & & V_\Sigma & 0 & 0 & V_1 & 0 & 0 \\ & & & & V_\Sigma & 0 & a & V_1 & 0 \\ & & & & & V_\Sigma & 0 & a & V_1 \\ & & & & & & V_\Pi - a & 0 & 0 \\ & & & & & & & V_\Pi & 0 \\ & & & & & & & & V_\Pi + a \end{bmatrix} \quad (11)$$

The first representation allows one to appreciate the effects of the SO coupling on the diabats. The diagonal elements of the matrix (8) are the SO-corrected diabats. The eigenvalues of this matrix will be referred to as the SO-corrected adiabats. The SO-corrected diabats are shown in Figure 10. The $|20\rangle$ diabat correlates with the lowermost state of the O(^{3}P$_J$) atom, $J = 2$, $M_J = 0$, whereas the $|00\rangle$ one correlates with the uppermost $J = 0$, $M_J = 0$ state. There are basically three types of shapes: a single T-shaped minimum, a double-minimum, and a nearly isotropic, shallow trough with two very weak minima. The T-shaped single-minimum diabats $|22+\rangle$, $|22-\rangle$, and $|10\rangle$ reflect the shape of the nonrelativistic V_Π diabat from which they originate (see matrix (8)). Among the double-minimum diabats, the $|20\rangle$ one has the deepest minimum corresponding to the $\Theta = 0°$, i.e., to the H-bonded configuration. All three shapes result from combining (to a varying degree) of V_Π and V_Σ spin-free potentials. Finally, $|00\rangle$, which is the least anisotropic, originates from an average nonrelativistic potential ($V_\Sigma + 2V_\Pi$). Such PES shapes are usually associated with rare gas-HCl interactions.[33]

The adiabatic SO-corrected potentials are shown in Figure 11. The five lowest adiabats correlate with the lowest state of the atom $J = 2$, and three of them (Figure 11: adiabats 1−3) have almost the same shape with the global minimum at $\Theta = 0°$ and the well depth 589 cm^{-1}. They closely resemble the lower spin-free $V_{1A''}$ adiabatic potential. The remaining potentials, shown in Figure 11 (adiabats 4 and 5), are nearly isotropic with the slight minimum on the non-H-bonded side. The lowest SO-corrected adiabat correlating with $J = 1$ (Figure 11, adiabat 6) has a T-shaped minimum. It resembles the A′ spin-free adiabat, but it is slightly deeper. The remaining potentials (7−9), including the uppermost (9) that correlates with $J = 0$, are again isotropic with a slight minimum (60−80 cm^{-1}) at $\Theta = 180°$. The SO adiabats (4, 5, 7, 8, 9) resemble the upper spin-free $V_{2A''}$ adiabat. In summary, the SO coupling has almost no effect on the shape of the lowest PES in O + HCl. This is in striking contrast with Cl + HCl where the SO coupling significantly reshapes the potential energy surfaces. However, the SO-coupling constant of Cl(^{2}P) is almost 1 order of magnitude larger than in O(^{3}P) (−588 cm^{-1} vs −77.5 cm^{-1}). The main effect of the SO in the case of O(^{3}P)−HCl is to split the nonrelativistic potentials into manifolds of closely spaced potentials, thereby providing multiple pathways for nonadiabatic processes.

Finally, the assumption of the independence of the SO parameter *a* on the geometry was also examined. To this end, the actual matrix elements of the Breit−Pauli H_{SO} Hamiltonian were evaluated for the three states considered here. The CASSCF calculations involved the fully uncontracted cc-pVTZ basis set, taking into account both one- and two-electron integrals of the Breit−Pauli operator.[23] The spin−orbit matrix element between nominally Σ and nominally (in-plane) Π states $\langle{}^3\Pi|H_{SO}|{}^3\Sigma\rangle$ (which correlates with the lowest state of the atom $J = 2$) is plotted in Figure 12 as a function of Θ for three distances. $R = 3.7$ Å roughly corresponds to the van der Waals minimum region, $R = 2.65$ Å to the region of the conical intersection on the H-bonded side, and $R = 2.25$ Å to the barrier region. The results indicate that in the region of the van der Waals well, and way up on the repulsive wall, the SO coupling remains fairly constant with geometry. Stronger variations occur at the H-bonded side, but even at $R = 2.25$ Å the difference in the SO coupling term between $\Theta = 0°$ and $\Theta = 180°$ is less than 100 cm^{-1}. The remaining matrix elements vary even less with geometry. It is therefore justified to assume that the *a* parameter remains constant in the pre-reactive region.

IV. Conclusions

Three adiabatic and four diabatic PESs have been obtained by combination of RCCSD[T] with MRCI calculations. Although the quantitative description of this interaction requires a high level of theory and a large basis set, the role of electrostatic interactions in shaping these potentials should be emphasized. The O(^{3}P) atom has more charge density along the doubly occupied p orbital, which results in the negative

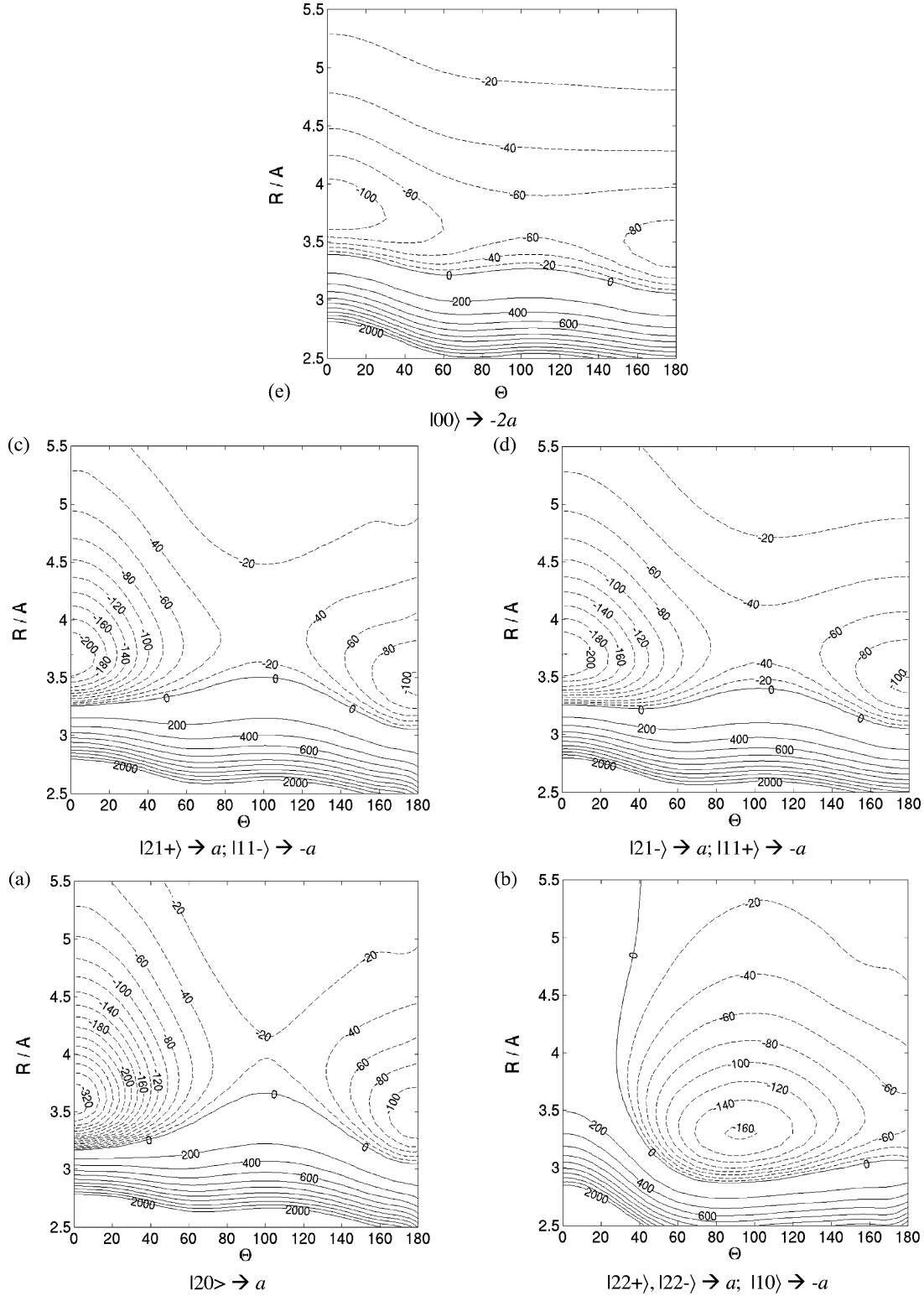

Figure 10. SO diabatic potentials of O + HCl (the asymptotic atomic limits are indicated by arrows).

quadrupole moment with respect to this axis. In the lowest adiabatic potential $^3A''$ the H-bonded minimum configuration ($R = 3.5$ Å, $\Theta = 0°$) results from a favorable orientation of the negative side of the quadrupole of O and the positive end of the dipole of HCl. In the upper $^3A''$ adiabatic potential the shallow minimum on the non-H-bonded side is due to the favorable orientation of the positive side of the quadrupole of O and the negative side of the dipole of HCl. Finally, the T-shaped well in the $^3A'$ adiabatic potential results from the quadrupole(O)−quadrupole(HCl) attraction. Clearly, the electrostatic effects act to orient the orbitals in the three states. A striking feature is the similarity between the shapes of the ab initio MRCI and multipole-derived coupling potential H_{12}. Given that most of our computational efforts were spent on the calculations of this potential, the possibility of replacing them with simple electrostatics is encouraging. The demonstrated electrostatic character of H_{12} gives justification to the model of Dubernet and Hutson,[34] which was applied in a number of

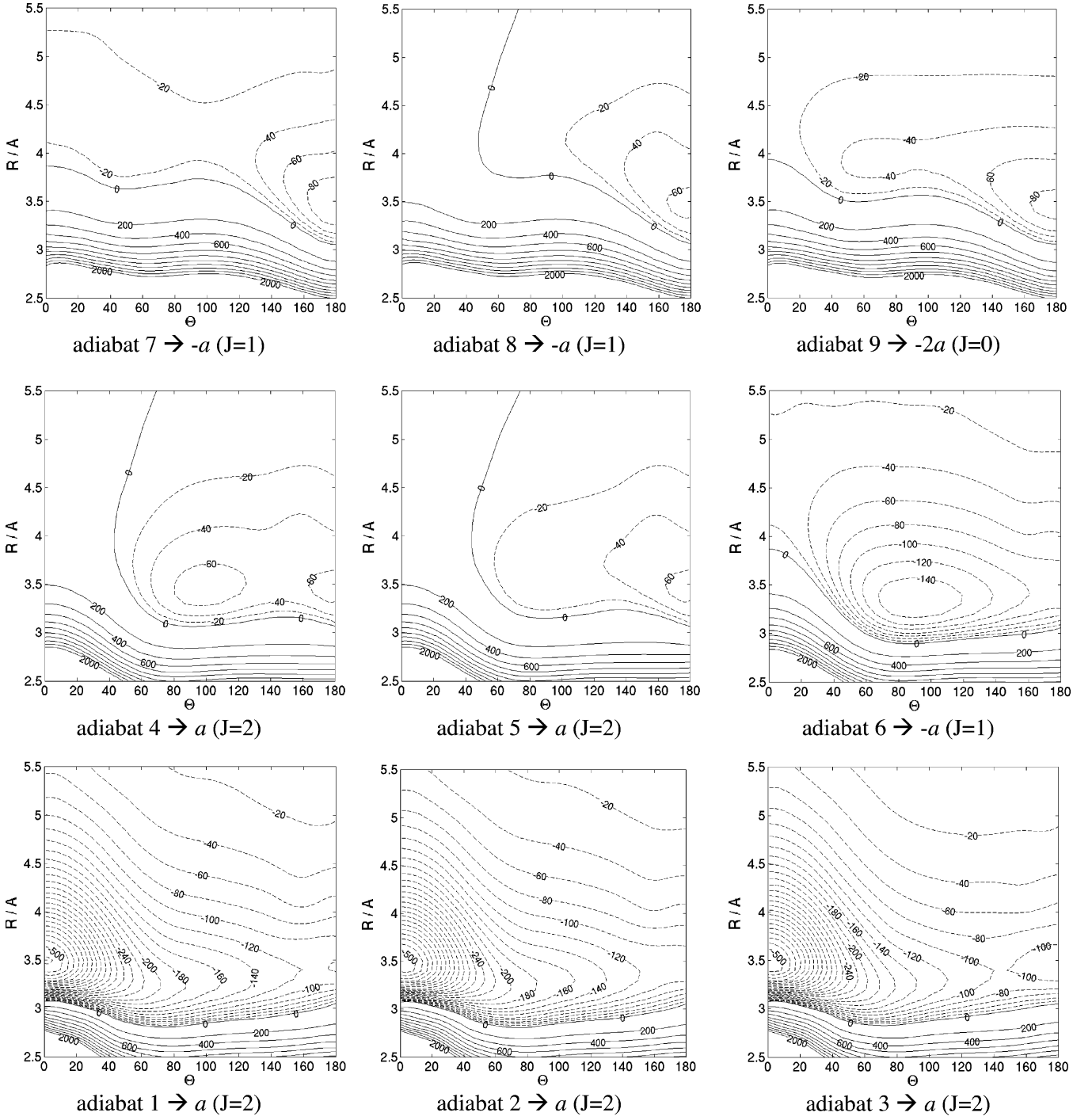

Figure 11. SO-corrected adiabatic potentials of O + HCl (asymptotic limits as indicated by arrows).

halogen atom−hydrogen halide pre-reactive complexes.[34−37] In the long-range $R > 5.5$ Å all three adiabatic and all diabatic potentials were obtained from electrostatic expressions.

There are three conical intersections of the adiabatic states Σ and Π in linear geometry: a single one in the short range on the H-bonded side, and a double crossing, the short and the long range, on the non-H-bonded side. The latter pair remains unaffected by the stretch of the intramonomer coordinate *r*. The two conical intersections on the non-H-bonded side are connected by a loop of avoided crossing that runs for slightly bent ($\Theta = 160-170°$) geometries. This is the region where the PESs are very difficult to calculate. It would be interesting to find out if and how these conical intersections affect the reaction probability below the reaction threshold. Previous reactive scattering calculations that detected a number of sharp resonances were performed on the single ground-state surface.[14] In the similar case of Cl + HCl, the conical intersection between Σ and Π surfaces (for $\Theta = 0°$) was implicated in the appearance of the Stueckelberg-type interference oscillations.[4]

The effects of SO coupling were investigated under the assumption of a constant SO parameter *a* throughout the van der Waals region. These effects are different from those in the related Cl + HCl complex. In Cl + HCl the SO coupling significantly reshapes the lowest nonrelativistic adiabatic potential, and in effect washes out a deep T-shaped minimum on the lowest $^2A'$ adiabat. In O + HCl the effects on the shape of the lowest adiabat are very small. The SO coupling splits the PESs into a manifold of 9 closely spaced potentials of varying shape. Ab initio calculations of the matrix elements of H_{SO}

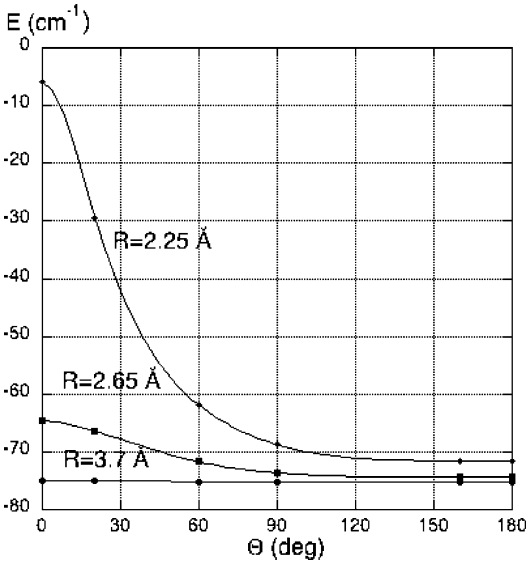

Figure 12. Dependence of the SO coupling between nominally Σ and in-plane Π states $\langle \Pi | H_{SO} | \Sigma \rangle$ on geometry in O + HCl.

between adiabatic states indicate that the SO parameter *a* can be considered constant in the entrance channel.

Acknowledgment. This work was supported by the National Science Foundation (Grants CHE-0414241 and CHE-0078533). A.A.B. also thanks Russian Basic Research Fund (Grant 05-03-32173).

References and Notes

(1) Schatz, G. C. *J. Phys. Chem.* **1995**, *99*, 7522 and references therein.
(2) Skouteris, D.; Manolopoulos, D. E.; Bian, W.; Werner, H.-J.; Lai, L.-H.; Liu, K. *Science* **1999**, *286*, 1713.
(3) Alexander, M. H.; Capecchi, G.; Werner, H.-J. *Science* **2002**, *296* 715. Manolopoulos, D. E. *Science* **2002**, *296*, 664.
(4) Schatz, G. C.; Hankel, M.; Whiteley, T. W. J.; Connor, J. N. L. *J. Phys. Chem. A* **2003**, *107*, 7278.
(5) Klos, J. A.; Chalasinski, G.; Szczesniak, M. M.; Werner, H. J. *J. Chem. Phys.* **2001**, *115*, 3085.
(6) Klos, J. A.; Chalasinski, G.; Szczesniak, M. M. *J. Chem. Phys.* **2002**, *117*, 4709.
(7) Klos, J. A.; Chalasinski, G.; Szczesniak, M. M. *Int. J. Quantum Chem.* **2002**, *90*, 1038.
(8) Klos, J. A.; Chalasinski, G.; Szczesniak, M. M. *J. Phys. Chem. A* **2002**, *106*, 7362.
(9) Klos, J.; Szczesniak, M. M.; Chalasinski, G. *Int. Rev. Phys. Chem.* **2004**, *23*, 541.
(10) Zeimen, W. B.; Klos, J.; Groenenboom, G. C.; Van der Avoird, A. *J. Phys. Chem. A* **2003**, *107*, 5110. See also: *J. Phys. Chem. A* **2004**, *108*, 9319.
(11) Zeimen, W. B.; Klos, J.; Groenenboom, G. C.; Van der Avoird, A. *J. Chem. Phys.* **2003**, *118*, 7340.
(12) Althorpe, S. C.; Clary, D. C. *Annu. Rev. Phys. Chem.* **2003**, *54*, 493.
(13) Skokov, S.; Tsuchida, T.; Nanbu, S.; Bowman, J. M.; Gray, S. K. *J. Chem. Phys.* **2000**, *113*, 227.
(14) Xie, T.; Wang, D.; Bowman, J. M.; Manolopoulos, D. E. *J. Chem. Phys.* **2002**, *116*, 7461.
(15) Koizumi, H.; Schatz, G. C.; Gordon, M. S. *J. Chem. Phys.* **1991**, *95*, 6421.
(16) Xie, T.; Bowman, J. M.: Peterson, K. A.; Ramachandran, B. *J. Chem. Phys.* **2003**, *119*, 9601.
(17) Ramachandran, B.; Schrader, E. A.; Senekowitsch, J. Wyatt, R. E. *J. Chem. Phys.* **1999**, *111*, 3862.
(18) Skokov, S.; Zou, S.; Bowman, J. M.; Allison, T. C. Truhlar, D. G.; Lin, B.; Ramachandran, B.; Garrett, B. C.; Lynch, B. J. *J. Phys. Chem. A* **2001**, *105*, 2298.
(19) Ramachandran, B.; Peterson, K. A. *J. Chem. Phys.* **2003**, *119*, 9590.
(20) Boys, S. F.; Bernardi, F. *Mol. Phys.* **1970**, *19*, 553: see also Alexander, M. H. *J. Chem. Phys.* **1993**, *99*, 6014.
(21) Szalay, P. G.; Gauss, J. *J. Chem. Phys.* **2000**, *112*, 4027.
(22) Chalasinski, G.; Szczesniak, M. M. *Chem. Rev.* **2000**, *100*, 4227.
(23) *Molpro* is a package of ab initio programs written by H. J. Werner and P. J. Knowles with contributions from J. Almlof, R. D. Amos, M. J. O. Deegan, S. T. Elbert, C. Hampel, W. Meyer, K. Peterson, E. A. Reinsch, R. Pitzer, A. Stone, and P. R. Taylor.
(24) Baer, M. *Chem. Phys. Lett.* **1975**, *35*, 112.
(25) Alexander, M. H. *J. Chem. Phys.* **1998**, *108*, 4467.
(26) Werner, H. J.; Knowles, P. J. *J. Chem. Phys.* **1988**, *89*, 5803.
(27) Rebentrost, F.; Lester, W. A. *J. Chem. Phys.* **1975**, *63*, 3737; **1975**, *64*, 3879.
(28) Dubernet, M. L.; Hutson, J. M. *J. Chem. Phys.* **1994**, *101*, 1939.
(29) Medved, M.; Fowler, P. W.; Hutson, J. M. *Mol. Phys.* **2000**, *98*, 453.
(30) Burcl, R.; Chalasinski, G.; Bukowski, R.; Szczesniak, M. M. *J. Chem. Phys.* **1995**, *103*, 1498.
(31) Moore, C. E. *Tables of Spectra of Hydrogen, Carbon, Nitrogen, and Oxygen*; Gallagher, J. W., Ed.; CRC Press: Boca Raton, FL, 1993.
(32) Buchachenko, A. A.; Jakowski, J.; Chalasinski, G.; Szczesniak, M. M.; Cybulski, S. M. *J. Chem. Phys.* **2000**, *112*, 5852. Buchachenko, A. A.; Szczesniak, M. M.; Chalasinski, G. *Chem. Phys. Lett.* **2001**, *347*, 415. See also: Aquilanti, V.; Grossi, G. *J. Chem. Phys.* **1980**, *73*, 1165.
(33) Chalasinski, G.; Szczesniak, M. M.; Kukawska-Tarnawska, B. *J. Chem. Phys.* **1991**, *94*, 6677. Chalasinski, G.; Szczesniak, M. M. *Chem. Rev.* **1994**, *94*, 1723.
(34) Dubernet, M. L.; Hutson, J. M. *J. Phys. Chem.* **1994**, *98*, 5844.
(35) Meuwly, M.; Hutson, J. M. *J. Chem. Phys.* **2000**, *112*, 592.
(36) Meuwly, M.; Hutson, J. M. *Phys. Chem. Chem. Phys.* **2000**, *2*, 441.
(37) Meuwly, M.; Hutson, J. M. *J. Chem. Phys.* **2003**, *119*, 8873.